Available online at www.sciencedirect.com
SCIENCE DIRECT
Surface Science 596 (2005) 12–20
SURFACE SCIENCE
www.elsevier.com/locate/susc

Metal nanostructure growth on molecular buffer layers of CO_2

P.S. Waggoner [a,c], J.S. Palmer [a,c], V.N. Antonov [b,c], J.H. Weaver [a,b,c,*]

[a] Department of Materials Science and Engineering, University of Illinois at Urbana-Champaign, 1304 West Green Street, Urbana, IL 61801, USA
[b] Department of Physics, University of Illinois at Urbana-Champaign, 1110 West Green Street, Urbana, IL 61801, USA
[c] Frederick Seitz Materials Research Laboratory, University of Illinois at Urbana-Champaign, 104 South Goodwin Avenue, Urbana, IL 61801, USA

Received 15 April 2005; accepted for publication 13 August 2005
Available online 15 September 2005

Abstract

Buffer-layer-assisted growth (BLAG) occurs when a multilayer of condensed gas acts as the surface on which impinging atoms form clusters that subsequently diffuse and coalesce during buffer desorption. We investigated Au, Cu, and Ni nanostructure formation using buffer layers of solid CO_2 and compared the results to what has been found for solid Xe buffers. The cluster densities could be controlled from $\sim 10^8$ to 10^{12} cm^{-2} by taking advantage of the power law dependence of density on the buffer layer thickness. For Au and Cu, the crossover from compact to ramified structures could be followed. For Ni, even small particles were ramified. The effective activation energies for diffusion of large ramified clusters on CO_2 were determined to be 0.91, 1.02, and 0.93 eV for Au, Cu, and Ni, respectively. These are significantly higher than those observed on Xe, and they reflect the higher polarizability of CO_2. The diffusion prefactors increased exponentially with the increase in diffusion barrier, demonstrating a Meyer–Neldel compensation effect. The characteristic energy of this process, 9 meV, was higher than for Xe due to the more energetic phonons of CO_2. It is comparable to the energies of buffer phonons active during buffer desorption, revealing that cluster motion on CO_2 is a many-body process fueled by coincidence of activated buffer phonons.

Keywords: Clusters; Growth; Surface diffusion; Carbon dioxide; Molecular solids

1. Introduction

There is much interest in the controlled synthesis of supported nanostructures of specific sizes and shapes, interest that is related to the novel

* Corresponding author. Tel.: +1 217 244 3528; fax: +1 217 333 2736.
E-mail addresses: pwaggone@uiuc.edu (P.S. Waggoner), jhweaver@uiuc.edu (J.H. Weaver).

0039-6028/$ - see front matter © 2005 Elsevier B.V. All rights reserved.
doi:10.1016/j.susc.2005.08.020

and potentially important properties of such structures. Recently, Huang et al. [1] introduced a technique for synthesis, based upon earlier work by Waddill et al. [2,3], that used a solid rare gas buffer layer to isolate the substrate from adatoms delivered by physical vapor deposition to the surface of the buffer. The weak interaction between the deposited material and the buffer allowed cluster nucleation, and the desorption of the buffer activated cluster diffusion and aggregation. This technique, termed buffer-layer-assisted growth or BLAG, is unique in that it avoids adatom interaction with the substrate and allows for the delivery of a wide range of pristine clusters on any given substrate.

BLAG was originally used to grow defect-free, abrupt metal–semiconductor interfaces [2,4]. Later, Huang et al. [1] recognized that the density of Ag particles delivered to Si(1 1 1)-(7 × 7) depended sensitively on the thickness of the buffer layer. Haley and Weaver [5] quantified this dependence and showed a power law dependence that agreed well with simulations of diffusion-limited cluster–cluster aggregation [6]. The physics of cluster diffusion on an incommensurate rare gas buffer was investigated by Antonov et al. [7,8] through studies of the growth of metal particles on Xe, Kr, and Ar. They demonstrated that cluster diffusivities varied as $D(S,T) = D(S)D(T)$ where $D(S)$ describes the cluster size dependence and $D(T)$ reflects the temperature dependence. Significantly, $D(S)$ was inversely proportional to the particle–buffer contact area S. The effective activation energies and pre-exponential factors associated with $D(T)$ were determined for clusters of several different metals on Xe, and a compensation effect [9] was discovered that related the energies and the pre-factors. Particle diffusion was then ascribed to many-body processes with the phonons of the buffer providing the needed energy.

In this paper, we focus on BLAG where the buffer layer is solid carbon dioxide and the nanostructures of interest are Au, Cu, and Ni. This extends previous work to a molecular buffer to demonstrate a broader generality of the technique. It also determines similarities and differences associated with higher desorption temperatures, a more complex metal–buffer interface, and lower symmetry in the solid buffer. As discussed below, the observed dependence of cluster number density on buffer layer thickness was strikingly similar to those found for BLAG on rare gas buffers. Pre-exponential factors for diffusion were several orders of magnitude larger than those for Xe, while effective activation energies were also larger by about a factor of 2. As observed in metal cluster diffusion on Xe [8], we find an exponential dependence of these pre-factors on activation energy that reflects the phonon energies of solid CO_2 activated during buffer desorption at ~90 K. Our results suggest that buffer materials that desorb at even higher temperatures than CO_2 may also give rise to nanoparticle formation.[1]

2. Experiment

Sample growth was done in a chamber operating at base pressures of $<1 \times 10^{-10}$ Torr. The substrates were 20–30 nm films of amorphous carbon (a-C) supported by Cu grids. They were cooled to ~20 K using a closed-cycle He refrigerator. The temperature was measured with a AuFe–Chromel thermocouple attached to the cold head. The buffer growth rate was determined from $I = p/(2\pi mkT)^{1/2}$ where I is the flux of incident molecules per unit time per unit area, p is the CO_2 partial pressure of 1×10^{-6} Torr, m is the molecular mass, and T is ambient temperature. The sticking coefficient was assumed to be unity, and the thickness was controlled by the time of exposure. Once the buffer was formed, the metals were vapor deposited from resistively heated sources (W baskets for Au and Cu and alumina-coated W baskets for Ni) with typical deposition rates of 0.02–0.05 Å/s. The amount deposited was measured with a quartz microbalance. While the amount is given in Ångstroms, referenced to the bulk parameters of the metals, we emphasize that the deposited

[1] Growth of a CO_2 buffer on a liquid nitrogen cooled substrate at 80 K would be possible at much higher partial pressures than used here, but this dynamic equilibrium would most likely have a deleterious effect on BLAG. In previous studies with Ar buffers, we found that 20 K was an upper limit for BLAG, with desorption at 35–40 K.

atoms formed clusters and did not wet the buffer layer.

After growth and warm up to room temperature, the samples were transferred through air to a Philips CM12 120 kV transmission electron microscope (TEM). Imaging was done in bright field mode, and the low intensity electron beam used did not appear to perturb the clusters. Samples stored in air were stable, and there were no changes in particle density or appearance. Cluster densities were determined directly from the TEM images with each connected structure considered to be one cluster, regardless of whether it was compact or ramified.

3. Buffer layer considerations

Solid CO_2 consists of linear, non-polar molecules loosely bound by van der Waals forces. It forms in the cubic *Pa3* structure below pressures of 11 GPa [10]. The lattice constant of solid CO_2 is 5.55 Å at 20 K, and the C=O bond length is 1.16 Å [11]. As shown in Fig. 1(a) and (b), carbon atoms reside on fcc lattice points, and the molecular axes are arranged to give the *Pa3* symmetry [12]. The buffer layer was assumed to grow with (1 1 1) texture since these planes have the highest planar density of molecules. The (1 1 1) surface is uneven since the 'up' O atoms on orthogonal CO_2 molecules extend 1.16 Å above the plane of C atoms. Solid CO_2 differs in both crystalline structure and surface structure from rare gas buffers which have close packed (1 1 1) surfaces.

The interfaces formed between the growing metal particles and the buffer are highly incommensurate with 36%, 53%, and 57% lattice mismatches for Au, Cu, and Ni, respectively. The lattice mismatch between Au(1 1 1) and CO_2(1 1 1) is shown in Fig. 1(c), where open circles correspond to Au atoms and filled circles represent the 'up' oxygen atoms. Clearly, the contact of the metals with CO_2 is poor and there should be little change in the interaction potential energy when particles are displaced on the surface. Thus, the barrier for diffusion should be small, as for Au–Xe where the mismatch was 51%.

Cluster diffusion and aggregation occurred during desorption of the CO_2 buffer. Once the He refrigerator was turned off, the warm up rate to room temperature, β, was 1.6 K/min, as in similar studies of rare gas desorption [8]. The desorption kinetics can be described by

$$\theta(t) = \int_0^t A \exp(-\varepsilon_{\mathrm{coh}}/k(\beta t'))\,\mathrm{d}t', \tag{1}$$

where $\theta(t)$ is the thickness of buffer that has desorbed at time t, A is $\sim 1\times 10^{16}$ (calculated from sublimation pressures in Ref. [11]), and $\varepsilon_{\mathrm{coh}}$ is the cohesive energy of CO_2, which is 0.272 eV [11]. CO_2 desorption occurs between 85 and 95 K. This compares to ~70–80 K for Xe. Though both have a 10 K desorption window, the use of CO_2 extends the upper temperature at which diffusion and aggregation can occur on the buffer. Thus, cluster diffusion and aggregation should be enhanced.

4. Results and discussion

A key parameter in rare gas BLAG was the buffer layer thickness because cluster diffusion and aggregation occurred on the desorbing layer. To study cluster growth on CO_2, we grew metal clusters on buffers ranging in thickness from 4 to 120 ML and compared them to clusters grown on similar thicknesses of Xe. Four monolayer buffers were sufficiently thin that clusters had little opportunity to diffuse and coalesce during desorption, thus representing the starting point prior to diffusion for clusters of a particular metal on a buffer of any thickness [7].

Fig. 2 shows TEM images obtained after depositing 5 Å on 4 ML CO_2. For Au and Cu, approximately spherical clusters are produced with 4–5 nm mean diameters (approximately 3000–4000 atoms per cluster) and cluster densities of 1.0–1.4×10^{12} cm^{-2}. The compact shape indicates that adatoms attaching to a growing cluster are able to diffuse to achieve a quasi-equilibrium structure with a decreasing surface to volume ratio. In contrast, the results for Ni showed particles with approximately three times the number of atoms per cluster and about one third of the density. These clusters were ramified rather than compact,

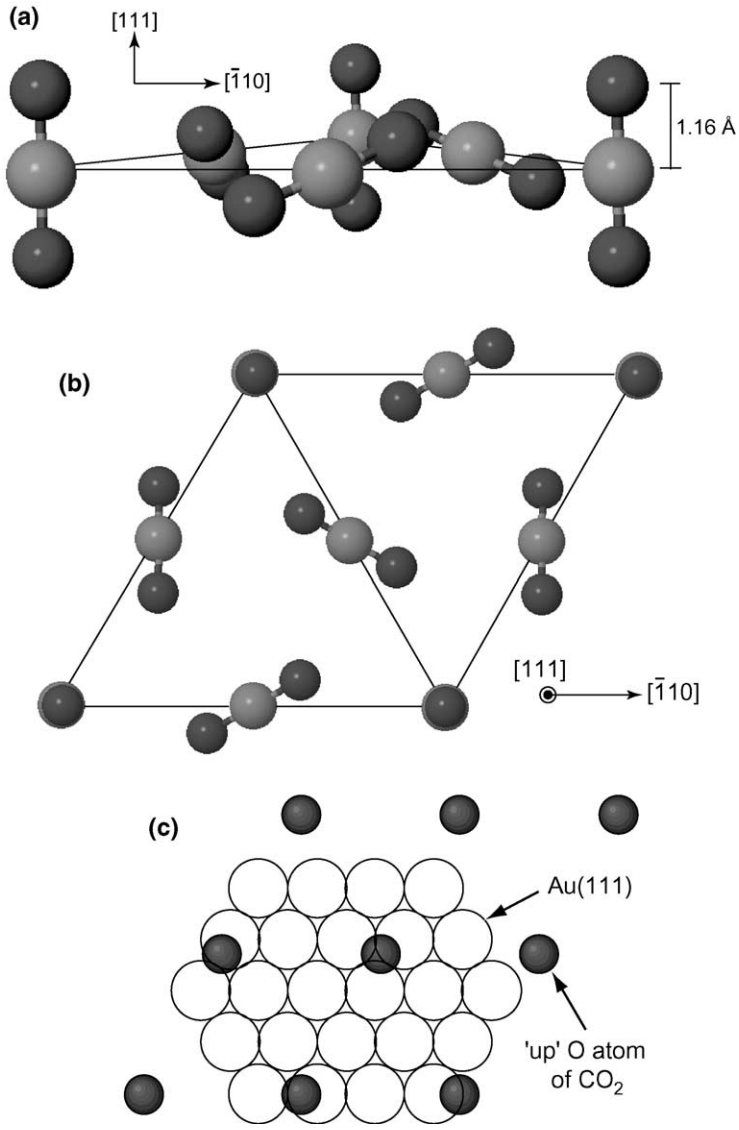

Fig. 1. Surface structure of CO_2(1 1 1) as viewed from the side (a) and from above (b). Carbon atoms occupy fcc lattice points, corner molecules are aligned perpendicular to (1 1 1), and molecules lying on $\langle\bar{1}10\rangle$ edges are oriented 35.26° inward from the plane edge and 19.5° above the (1 1 1) plane. This plane contains all four possible orientations in the *Pa3* crystal structure, with molecular axes parallel to $\langle 111\rangle$. Created from WebEMAPS Software [12] using crystal parameters from Ref. [11]. (c) A sketch of the interface formed between Au(1 1 1) and CO_2(1 1 1) layers showing a poor lattice match. The smaller, filled circles represent 'up' O atoms from perpendicular CO_2 molecules and the larger, open circles represent Au atoms. The radii are proportional to the atomic radii of O and Au. The nearest neighbor distances for Au and 'up' CO_2 molecules are 2.89 Å and 7.85 Å, respectively.

with arm widths typically ranging from 2 to 3.5 nm. Ramified clusters were also observed for Ni deposited on 4 ML Xe, indicating that Ni diffusion on Ni is insufficient at low temperatures to form compact particles. We note that simulations of surface self-diffusion for transition metals have predicted activation barriers on Ni(1 1 1) to be significantly larger than Au(1 1 1) and Cu(1 1 1) [13]. Although surface diffusion pathways underlying the coalescence of evolving clusters formed via BLAG are

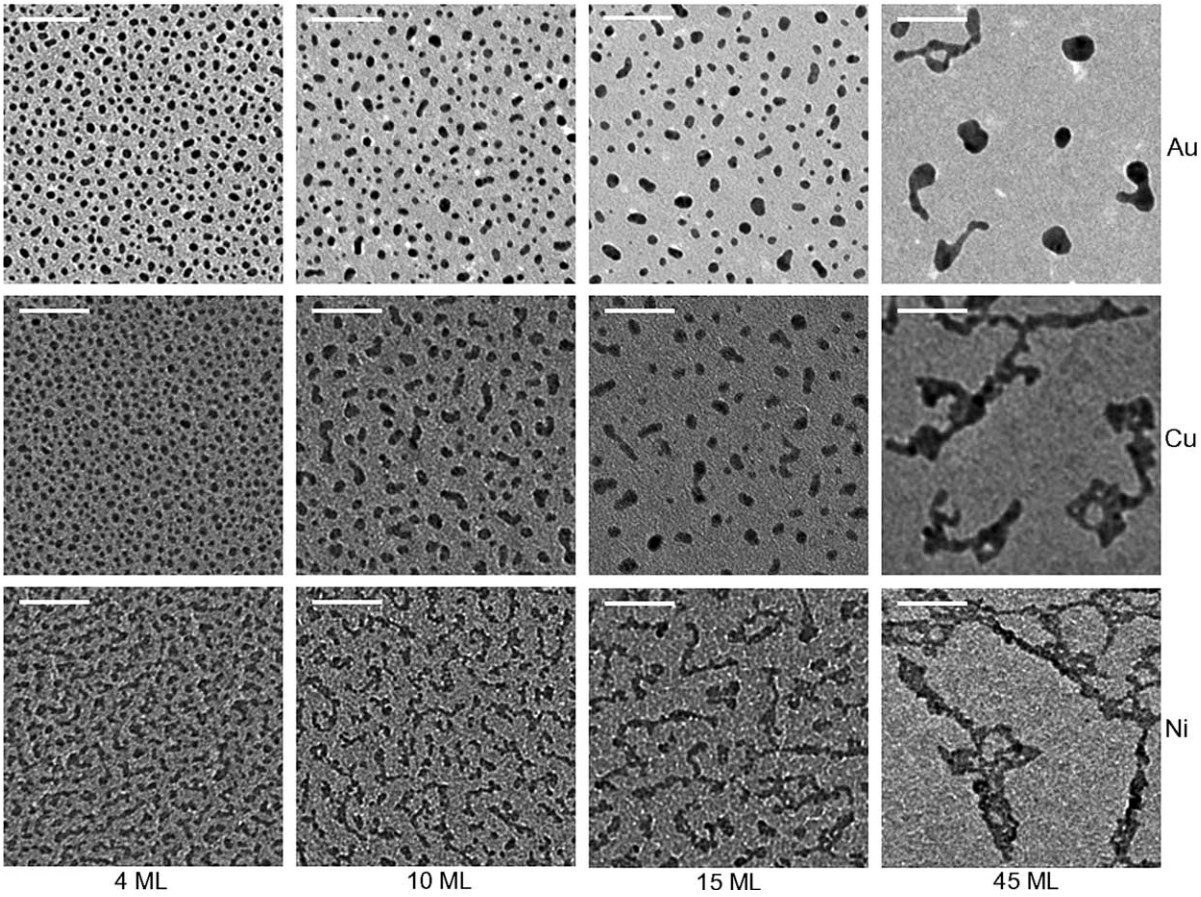

Fig. 2. TEM micrographs of Au, Cu, and Ni clusters grown on buffers of 4, 10, 15, and 45 ML in thickness; all images are 200×200 nm with 50 nm scale bars. Cluster densities, $\langle n \rangle$, were calculated directly from images like those shown to determine the dependence of $\langle n \rangle$ upon buffer layer thickness. A contiguous cluster was counted as a single unit, regardless of whether it was compact or ramified.

complicated, these simulations may give some insight into the reduced coalescence of Ni clusters.

In discussions of coalescence on rare gas solids, we speculated that the particles would be coated with a monolayer of rare gas to lower their surface energies [5]. Similarly, we reason that CO_2 also coats the surface of these particles since CO_2 physisorption has been reported on Au, Cu, and Ni surfaces at 80–120 K [14]. We see the same particle patterns for growth on CO_2 and Xe buffers and conclude that adatom attachment and diffusion on a growing cluster is not significantly impeded by the presence of CO_2. As a counterexample, we note that Pd growth on Xe produced compact clusters, while the same system exposed to a capping layer of CO gave rise to a much more ramified structure. This effect can be understood by the tendency of CO to chemisorb, carbon atom down, on Pd surfaces, which therefore limits surface diffusion and coalescence [15].

The TEM images of Fig. 2 show changes in the particle appearance for 5 Å metal deposited as the buffer thickness increased from 4 to 45 ML. For buffers of 10 or more monolayers, the Au clusters had the highest density, while Ni clusters had the lowest density and were the most ramified. Ni growth on buffers of ~60 ML or more resulted in a single percolated network. The rather large surface coverage for Ni plays a major role in creating this network on such a thin layer of CO_2. For Au

and Cu, percolated networks have not yet formed at 120 ML and 90 ML, respectively, but should eventually. An alternate way to produce such a network is to increase the amount of metal deposited because the surface coverage increases. Indeed, we observed a percolated network after depositing 50 Å of Au on 60 ML CO_2. At this point the surface coverage was 50.7%, and the average thickness was ~99 Å. It is likely that the network was formed on the buffer and desorption had relatively little effect.

The surface coverage, ρ, changes with buffer layer thickness, decreasing steadily when the clusters can coalesce completely (3D growth). It becomes constant after cluster growth becomes ramified (2D growth), which happens when the particles reach a critical size, above which the time scale of coalescence is large compared to the time scale of aggregation [16]. This crossover is relatively abrupt because the coalescence rate at a given temperature decreases exponentially with particle size [17]. For 5 Å of Au on CO_2, ρ stabilizes at 8.5% for growth on buffers of ~90 ML thickness, as determined from TEM images. It leveled off at 12% and 20% for Cu and Ni, respectively, for ~45 ML buffers for each metal. These are all lower coverages than for an equivalent amount of material deposited on Xe, namely 12%, 16%, and 22% [8]. The difference can be attributed to the fact that aggregation happens at the higher desorption temperature of CO_2 compared to Xe, at which the typical crossover size is larger. Since coalescence is essentially a surface diffusion process, it is interesting to note that the ordering of these constant coverages on both Xe and CO_2 matches the ordering of surface self-diffusion activation barriers on (1 1 1) surfaces, increasing from Au to Cu to Ni [13].

The fact that surface coverage is affected by the desorption temperature of the buffer seems to be a general effect since stabilized surface coverages decrease from 13.5 to 13, 12, and 8.5% for Ar, Kr, Xe, and CO_2, respectively, in order of increasing desorption temperature.[2] This relationship will be discussed further later in this paper. This trend implies that the structures are stable on the substrate surface and post-delivery coalescence at room temperature is insignificant for ramified structures far from equilibrium.

For rare gas buffers, cluster growth proceeded via diffusion-limited cluster–cluster aggregation (DLCCA), and ramified islands eventually developed [5]. These ramified clusters exhibit a Hausdorff fractal dimension that relates the projected area of clusters with their average radius [18]. For our results, we deduced that the fractal dimensions were 1.50 ± 0.05, 1.55 ± 0.04, and 1.60 ± 0.03 for Au, Cu, and Ni, respectively. These values agree well with other studies of aggregated cluster fractal dimensions, confirming that buffer-layer-assisted growth on CO_2 occurred via DLCCA [5,15].

The cluster density, $\langle n \rangle$, reflects the diffusion parameters governing movement of the particles on the buffer. Comparing growth on CO_2 and Xe, we might expect that the higher temperature of desorption would enhance surface diffusion while stronger interaction with the buffer would reduce it. Fig. 3 shows how $\langle n \rangle$ depends on buffer thickness for each metal. As for rare gas buffers, the cluster densities exhibit a power law dependence on the buffer thickness, θ, in the form

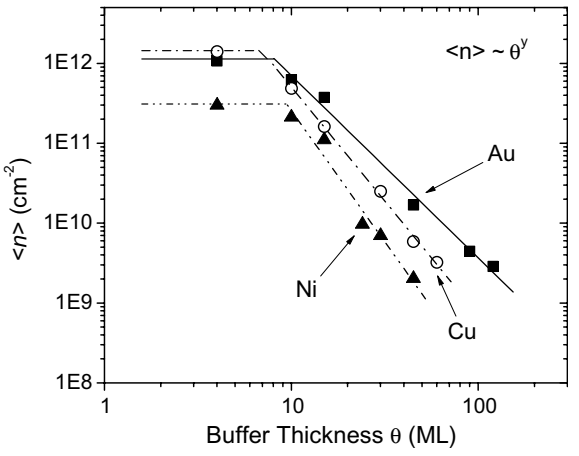

Fig. 3. Cluster density, $\langle n \rangle$, as a function of buffer layer thickness, θ. The slopes determine the exponent of decay defined in the figure, with $y = -2.28 \pm 0.12$ for Au, -2.85 ± 0.09 for Cu, and -3.28 ± 0.33 for Ni.

[2] Calculated from images collected in previous studies of Ar, Kr, and Xe in Refs. [7] and [8].

$\langle n\rangle \propto \theta^y$, where y was -2.28 ± 0.12, -2.85 ± 0.09, and -3.28 ± 0.33 for Au, Cu, and Ni, respectively. These exponents are comparable to those for these metals on Xe, namely -2.41 ± 0.09, -2.34 ± 0.14, and -3.52 ± 0.20, respectively [8]. Thus, Au and Ni have slightly smaller decay rates and Cu has a faster, though still fairly similar, falloff on CO_2 than on Xe. From the similarity of y for the two buffers, we expect that the higher desorption temperature of CO_2 either has a negligible effect on cluster diffusion or that it is offset by a stronger interaction with the buffer.

To determine the effective activation energies for the diffusion of ramified clusters, we follow the protocol developed by Antonov et al. [8]. They used theoretical calculations of the density as a function of cluster diffusivity and time,

$$\langle n\rangle \propto (D_{S_0} t)^z \tag{2}$$

where D_{S_0} is the diffusivity of a particle with a contact area of S_0 and t is time [19]. Replacing $D_{S_0}t$ with a modified Arrhenius description of diffusivity that takes into account the warm-up rate of our system, β, lets us connect the cluster density with a diffusion pre-factor, D_{00}, and an effective activation energy, ε_d, for diffusion. The addition of β to the equation introduces time and an integral of the form $\int_0^t D_{00}\exp\{-\varepsilon_d/(k\beta t')\}\,dt'$. If $\langle n\rangle$ is determined experimentally for two buffer thicknesses, then the ratio of two equations for $\langle n\rangle$ of the form

$$\frac{\langle n(\theta_1)\rangle}{\langle n(\theta_2)\rangle} = \left[\frac{\left(\int_0^{t(\theta_1)} \exp\{-\varepsilon_d/(k\beta t')\}\,dt'\right)}{\left(\int_0^{t(\theta_2)} \exp\{-\varepsilon_d/(k\beta t')\}\,dt'\right)}\right]^z \tag{3}$$

eliminates D_{00} and leaves only a single unknown, ε_d. Here $t(\theta_n)$ is the time needed to desorb a buffer layer of thickness θ_n. The exponent z in Eqs. (2) and (3) was recently determined for 2D systems by simulating cluster coalescence in the ramified regime, with the result that $z = -0.5 - (2.46 \pm 0.03)\rho$ where ρ is the fractional surface coverage [8].

Solving Eq. (3) for the activation energy yields $\varepsilon_d = 0.91 \pm 0.05$ eV (Au), 1.02 ± 0.03 eV (Cu), and 0.93 ± 0.09 eV (Ni) for clusters grown from 5 Å depositions on CO_2. These activation energies are greater than those on Xe, namely 0.53 (Au), 0.46 (Cu), and 0.60 eV (Ni) [8], but they are still small considering that the ramified clusters are derived from tens of thousands of atoms. It should be noted that these *effective* activation energies are not barriers in the sense of surface diffusion where hopping occurs between local potential wells. Molecular dynamics simulations [20] of cluster diffusion on incommensurate surfaces have shown that cluster diffusion is Brownian-like and does not involve a corrugated surface potential. Since we find similar power law decays of cluster densities of Au, Cu, and Ni on Xe and CO_2 despite the significant increase in ε_d, we conclude that the increase in effective activation energy for clusters on CO_2 approximately offsets the increase in desorption temperature of the buffer.

For our buffer layers, the van der Waals bonding arises from the polarizability of the solid. The degree of polarizability directly determines bond strengths within the solid and is therefore directly related to the cohesive energy of the buffer. Similarly, we expect a greater polarizability of the buffer to result in stronger interaction with the metal particles, leading to higher effective activation energies of diffusion. Our results for increased activation energies on CO_2 match this reasoning since it has a higher cohesive energy than Xe. This relationship can be extended in order to connect buffer desorption temperature, depending explicitly on ε_{coh}, to the temperature at which cluster diffusion and aggregation occurs, related to ε_d. Therefore, the observed dependence of surface coverage on buffer desorption temperature is actually a dependence upon the temperature at which aggregation occurs, agreeing with the increasing degree of coalescence at higher temperatures discussed earlier.

Antonov et al. [8] were also able to determine diffusivities and the experimental pre-exponential factors, D_{00}, by comparison of the experimental results with those of a simulation of 2D coalescence using experimentally determined values for activation energy. The simulation unit cell size is assigned to the typical ramified cluster branch width (~10 nm), and real time is matched to simulation time by comparing simulated and experimental results for equivalent cluster densities. For Au, Cu, and Ni clusters with projected areas of 100 nm^2 on CO_2, comparison with the simula-

tion yields diffusion pre-exponents of 1.12×10^{31}, 1.19×10^{37}, and 2.35×10^{33} cm^2/s, respectively. These pre-factors are several orders of magnitude larger than the same metal clusters on Xe. Because diffusing particles do not experience a corrugated potential where hopping distances and attempt frequencies would be relevant [8,20] these pre-exponential values cannot be related to an attempt frequency. Such large values and their variations can be understood in terms of the Meyer–Neldel (MN) rule or the compensation effect [9]. For systems that obey the MN rule, the pre-exponent, $A(E)$, tracks the activation energy, E_d, through

$$A(E) \propto \exp(E_d/E_{MN}), \quad (4)$$

where E_{MN} is the characteristic Meyer–Neldel energy of the system. Yelon and Movaghar have argued that compensation effects arise in systems where the activation energy of a certain process is much larger than the elementary excitations of that system and kT [21,22]. The large number of elementary excitations required for a process introduces significant configurational entropy into the system and leads to the very large pre-factor. For BLAG on rare-gas solids, cluster diffusion has been shown to be a many-body process with buffer phonons as excitations and with the characteristic energy for metal cluster diffusion on Xe being comparable to the active acoustic phonon modes in Xe [8]. We expected a larger characteristic energy for CO_2 due to its more energetic phonons.

To determine whether an expression of the form of Eq. (4) was valid for diffusion on CO_2, we plotted $\ln(D_{00})$ vs. ε_d for Au, Cu, and Ni clusters, as shown in Fig. 4. Calculating the slope of this line yields a characteristic energy of 9 ± 2 meV. This compares to 6.9 meV for diffusion on Xe [8]. At 88 K, there are three major phonon modes active with energies of 9.05, 11.2, and 16.2 meV with relative intensities of 100, 24, and 10, respectively [23]. E_{MN} agrees very well with the energies of the most prominent phonons, demonstrating the key role that phonons play in diffusion on CO_2. Thus, we conclude that cluster diffusion on CO_2 is a phonon-activated process requiring the superposition of a large number of buffer phonons to activate cluster motion.

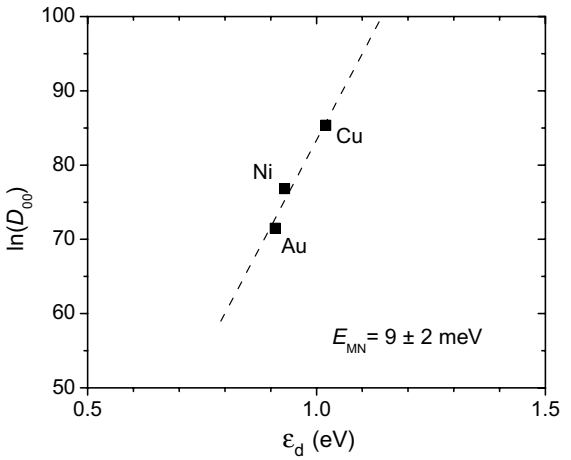

Fig. 4. Diffusion pre-exponents, D_{00}, as a function of effective activation energy for cluster diffusion, ε_d, for Au, Cu, and Ni clusters on CO_2, showing that an increase in the activation energy is compensated by an exponential increase in D_{00}. The slope of the line is the inverse of the Meyer–Neldel characteristic energy, E_{MN}, which was determined to be 9 ± 2 meV. This energy compares well to the active phonon excitations at the temperature range of CO_2 desorption, 85–95 K.

5. Conclusions

In this work, we focused on the feasibility of BLAG on a molecular solid, CO_2, and found that the general principles underlying cluster growth and diffusion are transferable to molecular buffers. The observed power law dependence of cluster density on buffer thickness and fractal dimension of ramified clusters indicates diffusion limited cluster–cluster aggregation. Effective activation energies for cluster diffusion on CO_2 were on the order of 1 eV, about a factor of 2 higher than for diffusing metal particles on Xe, and the difference can be attributed to a stronger interaction of these metal clusters with CO_2. We find competition between the increased temperature of desorption and the stronger binding of clusters to the buffer, in terms of effective activation energies. These effects appear to offset each other while reducing surface coverage due to increased coalescence at higher desorption temperatures. The pre-exponential factors, D_{00}, exhibit a compensation effect, increasing exponentially with the effective activation energy for cluster diffusion. The characteristic Meyer–Neldel energy compares very well with the

prominent active phonon modes during buffer desorption, demonstrating the many-body nature of phonon-stimulated cluster diffusion on desorbing molecular buffers. We expect similar effects for all buffers suitable for BLAG.

Acknowledgments

This work was supported by the US Department of Energy Division of Materials Sciences under Grant No. DEFG02-01ER45944. The experiments made use of facilities within the Center for Microanalysis of Materials at the Frederick Seitz Materials Research Laboratory which is supported by DOE Grant DEFG02-91ER45439. P.S.W. was supported by the NSF research experience for undergraduates program and an AVS undergraduate research award. We thank P. Swaminathan for useful discussions.

References

[1] L. Huang, S.J. Chey, J.H. Weaver, Phys. Rev. Lett. 80 (1998) 4095.
[2] G.D. Waddill, I.M. Vitomirov, C.M. Aldao, J.H. Weaver, Phys. Rev. Lett. 62 (1989) 1568.
[3] G.D. Waddill, I.M. Vitomirov, C.M. Aldao, S.G. Anderson, C. Capasso, J.H. Weaver, Phys. Rev. B 41 (1990) 5293.
[4] J.H. Weaver, G.D. Waddill, Science 251 (1991) 1444.
[5] C. Haley, J.H. Weaver, Surf. Sci. 518 (2002) 243.
[6] P. Meakin, T. Vicsek, F. Family, Phys. Rev. B 31 (1985) 564.
[7] V.N. Antonov, J.S. Palmer, A.S. Bhatti, J.H. Weaver, Phys. Rev. B 68 (2003) 205418.
[8] V.N. Antonov, J.S. Palmer, P.S. Waggoner, A.S. Bhatti, J.H. Weaver, Phys. Rev. B 70 (2004) 045406.
[9] W. Meyer, H. Neldel, Z. Tech. Phys. (Leipzig) 12 (1937) 588.
[10] K. Aoki, H. Yamawaki, M. Sakashita, Y. Gotoh, K. Takemura, Science 263 (1994) 356.
[11] V.G. Manzhelii, Y.A. Freiman (Eds.), Physics of Cryocrystals, AIP Press, Woodbury, NY, 1997.
[12] J.M. Zuo, J.C. Mabon, WebEMAPS Software, University of Illinois at Urbana, Champaign, URL: http://emaps.mrl.uiuc.edu/.
[13] C.L. Liu, J.M. Cohen, J.B. Adams, A.F. Voter, Surf. Sci. 253 (1991) 334.
[14] H.-J. Freund, M.W. Roberts, Surf. Sci. Rep. 25 (1996) 225.
[15] V.N. Antonov, J.H. Weaver, Surf. Sci. 526 (2003) 97.
[16] B. Yoon, V.M. Akulin, Ph. Cahuzac, F. Carlier, M. de Frutos, A. Masson, C. Mory, C. Colliex, C. Bréchignac, Surf. Sci. 443 (1999) 76.
[17] N. Combe, P. Jensen, A. Pimpinelli, Phys. Rev. Lett. 85 (2000) 110.
[18] P. Meakin, Phys. Rev. Lett. 51 (1983) 1119.
[19] M. Kolb, Phys. Rev. Lett. 53 (1984) 1653.
[20] P. Deltour, J.-L. Barrat, P. Jensen, Phys. Rev. Lett. 78 (1997) 4597.
[21] A. Yelon, B. Movaghar, Phys. Rev. Lett. 65 (1990) 618.
[22] A. Yelon, B. Movaghar, H.M. Branz, Phys. Rev. B 46 (1992) 12224.
[23] J.E. Cahill, G.E. Leroi, J. Chem. Phys. 51 (1969) 1324.